






## RESEARCH ARTICLE

# LAX phases: A family of novel stable layered materials, informatics-based discovery

Ehsan Alibagheri<sup>1</sup>  | Mohammad Khazaei<sup>1,2</sup>  | Mehdi Estili<sup>3</sup>  |  
Alireza Seyfi<sup>1</sup> | Hiroshi Mizoguchi<sup>4</sup> | Kaoru Ohno<sup>5</sup> | Hideo Hosono<sup>4,6</sup>  |  
S. Mehdi Vaez Allaei<sup>1,7</sup> 

<sup>1</sup>Department of Physics, University of Tehran, Tehran, Iran

<sup>2</sup>School of Nano Science, Institute for Research in Fundamental Sciences (IPM), Tehran, Iran

<sup>3</sup>Research Center for Electronic and Optical Materials, National Institute for Materials Science (NIMS), Tsukuba, Ibaraki, Japan

<sup>4</sup>Research Center for Materials Nanoarchitectonics (MANA), National Institute for Materials Science (NIMS), Tsukuba, Ibaraki, Japan

<sup>5</sup>Department of Physics, Yokohama National University, Yokohama, Japan

<sup>6</sup>MDX Research Center for Element Strategy, International Research Frontiers Initiative, Yokohama, Japan

<sup>7</sup>New Uzbekistan University, Tashkent, Uzbekistan

## Correspondence

Ehsan Alibagheri, Mohammad Khazaei, and S. Mehdi Vaez Allaei, Department of Physics, University of Tehran, North Kargar Avenue, Tehran 14395-547, Iran.  
Email: [e.alibagheri@ut.ac.ir](mailto:e.alibagheri@ut.ac.ir), [mohammad.khazaei@ut.ac.ir](mailto:mohammad.khazaei@ut.ac.ir), and [smvaez@ut.ac.ir](mailto:smvaez@ut.ac.ir)

## Funding information

Iran National Science Foundation, Grant/Award Number: 4025794; Japan Society for the Promotion of Science, Grant/Award Number: 24K08211

## Abstract

Ternary MAX phases, characterized by the chemical formula  $M_2AX$ , represent a group of layered materials with hexagonal lattices. These MAX phases have been the subject of extensive experimental and theoretical studies. Formation energy and thermodynamic calculations indicate that MAX phases containing late transition metals, such as Rh, Ru, Pt, Pd, Co, and Ni, are unlikely to form. Here, we introduce an alternative family of orthorhombic and monoclinic materials, the LAX phases, which exhibit similarities to MAX phases in terms of their layered structure and A and X elements. However, LAX materials incorporate late transition metals in place of the early transition metals. Advanced techniques for predicting the crystal structure of materials, coupled with data-driven materials research and machine learning algorithms, were employed to investigate the stable structures containing transition metals from the last groups of the d-block elements. The analyses revealed 207 ternary LAX systems that demonstrate robust stability against decomposition, with 100 of these systems showing dynamic stability. An in-depth examination of the top 10 structures revealed five LAX systems that are phase stable and exhibit superior mechanical properties, outperforming MAX phase counterparts in Young's modulus, stiffness, and hardness. These findings indicate that many LAX phase structures are viable candidates for future synthesis, highlighting the potential of heuristic-based structure searches in material discovery.

## KEYWORDS

evolutionary algorithm, LAX phases, machine learning, materials discovery, materials informatics, MAX phases

## 1 | INTRODUCTION

The study of layered materials represents a long-standing and intriguing area of research within the field of materials science. Graphite and MAX phases are the most widely recognized materials in this field. Graphite exhibits interlayer bonding via van der Waals forces, whereas MAX phases constitute a distinct group of layered crystals with covalent and/or metallic interlayer interactions. MAX phases were initially discovered in the 1960s and are described by the chemical formula  $M_{n+1}AX_n$  where M is an early transition metal (Sc, Ti, Zr, Hf, V, Nb, Ta, Cr, and Mo), A is an element from groups 13–16 (e.g., Al, Ga, In, Bi, and Tl), and X can be carbon or nitrogen.<sup>1</sup> MAX phases are composed of block layers of  $M_{n+1}X_n$  interleaved with layers of the A-group elements.<sup>2–8</sup> In addition to the MAX phases, a number of other layered materials have been the subject of extensive investigations, each offering distinctive exotic properties.<sup>9–11</sup> Over the past 20 years, MAX phases have attracted significant attention from the materials science community due to their unique combination of metallic- and ceramic-like properties. These phases are distinguished by their adaptability in elemental composition and crystal engineering while maintaining a layered structure.<sup>12–21</sup> This characteristic has led to the development of various innovative MAX phase structures, including out-of-plane double transition metals MAX phases, in-plane double transition metals MAX phases,<sup>22</sup> high-entropy alloy MAX phases,<sup>23</sup> and superlattice MAX phases.<sup>24</sup> While the majority of MAX phase compounds exhibit metallic characteristics, a few semiconducting MAX phases have been proposed in the theoretical literature.<sup>25</sup> The fascination with this class of materials lies not only in their rich chemistry and layered structure, but also in their mechanical properties. They offer a distinctive combination of high-temperature strength, damage tolerance, and thermal shock resistance, rendering them highly desirable for a multitude of industrial applications.<sup>5,26–28</sup> Understanding and optimizing the mechanical behavior of MAX phases is crucial for enhancing their performance and expanding their application in sophisticated systems.

The selection of early transition metals, such as scandium, titanium, vanadium, or chromium, which possess varying atomic radii, valence electron numbers, and oxidation states, can influence the mechanical, electronic, and magnetic properties of the resulting MAX phases.<sup>2,29,30</sup> These metals, typically found in groups IV–VI of the periodic table, possess a unique combination of properties that make them ideal candidates for forming robust and stable structures that are characteristic of MAX phases. The capacity of MAX phases to accommodate a range of A-group elements while maintaining structural integrity

further enriches their chemical compositions, thereby enhancing their exotic properties for potential applications in sophisticated technologies.<sup>29,31–36</sup> The recent progress in adding and predicting new M, A, and X elements is attractive for achieving additional new members in this family.<sup>37,38</sup> Early transition metals are commonly employed as the M elements in MAX phase structures, whereas middle and late transition metals are less widely used. This can be attributed to a number of factors, including the number of valence electrons, the atomic radii of the M, A, and X elements, and the bond strength in M–X and M–A bonds. Additionally, the existence of stable competitive crystals with the same stoichiometry may also play a role. In MAX phases, the strong M–X bonds play a pivotal role in enhancing the structural stability of these materials. Essentially, the  $M_{n+1}X_n$  blocks serve as the fundamental building blocks of MAX phases. Beyond their composition and structure, the mechanical properties of MAX phase materials represent a significant area of interest and exploration.<sup>39–45</sup>

By utilizing computational algorithms and data-driven models, researchers can accelerate the exploration and development of new MAX phases with customized properties.<sup>46,47</sup> The analysis of structures and the identification of potential candidates for diverse technological applications are enabled by machine learning (ML) models trained on chemical datasets.<sup>34,48–50</sup> The efficacy of ML algorithms in tackling physics-related problems is evident, particularly in their effectiveness in classification and regression models, which depend on the desired properties.<sup>51–57</sup>

In order to propose a novel structure for MAX phases containing middle and late transition metals, we conducted a comprehensive analysis of the dynamic stability of MAX phases composed of late transition metals that exhibit negative phonon frequencies. Using the phonon eigenvectors of the negative phonon modes of these structures, we developed modulated structures of MAX phases. Our detailed analysis led to the discovery of an orthorhombic and monoclinic lattice structure with symmetry groups 59 (Pmmn) and 11 (P2<sub>1</sub>/m), respectively, which resembles the layered structure of MAX phases, as depicted in Figure 1. Two analogous structures (Ni<sub>2</sub>InP<sup>58</sup> and Ni<sub>2</sub>SnP<sup>59</sup>) were previously synthesized with symmetry groups 13 (P2/c) and 62 (Pnma), respectively. The two structures have different lattice parameters and are situated along the stability line with LAX structures. The novel structure exhibited enhanced energetic stability in comparison to the original MAX phase structure and did not display any negative phonon modes. Henceforth, we will refer to these structures as LAX phases, which exhibit similarities to MAX phases but utilize late or middle transition metals.

In order to ascertain the reliability of our proposed LAX design as a viable choice for MAX phases containing

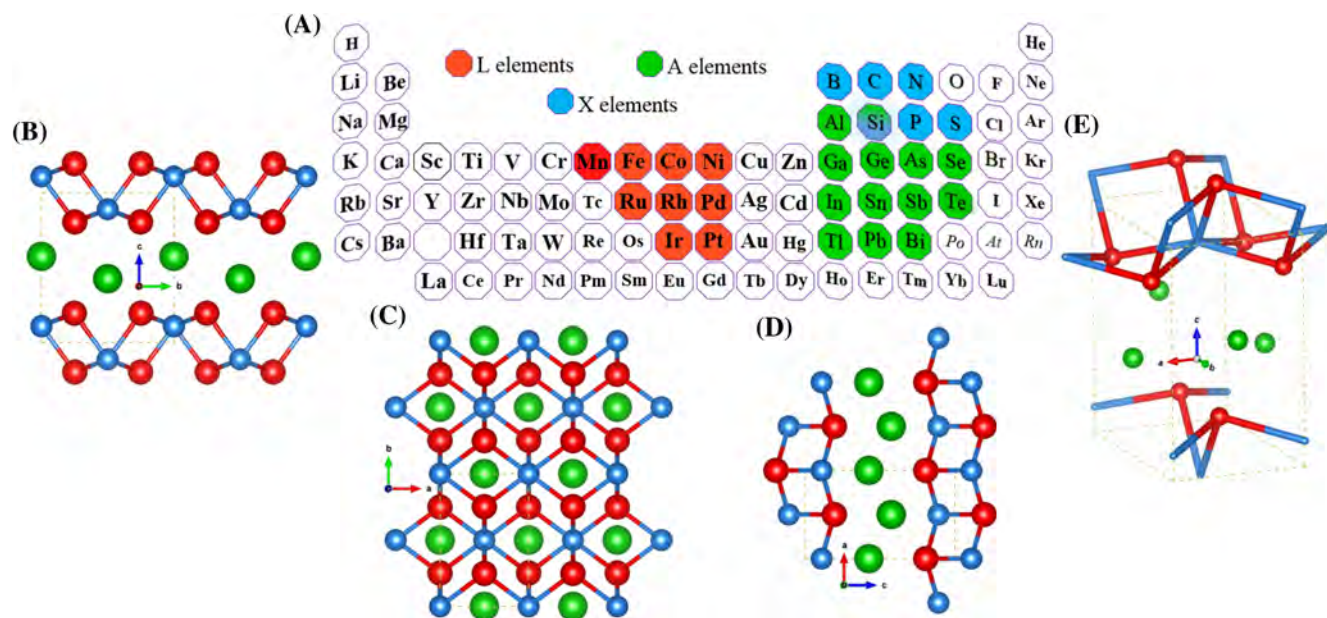


**FIGURE 1** Crystal structure and composition window of the discovered LAX phases. (A) The elements utilized, such as L, A, and X, are highlighted. (B–D) The 4–2–2 structures from directions of 1–0–0, 0–0–1, and 0–1–0, respectively. (E) A 3D illustration of the unit cell.

middle or late transition metals, we have conducted an exhaustive search of our compiled dataset of 702 ternary  $L_2AX$  structures. Computational algorithms and data-driven models were employed to expedite the investigation of synthesizable  $L_2AX$  phases. In particular, ML models trained on chemical datasets are utilized to analyze structures and identify potential candidates. Upon comparing the MAX and LAX phases with similar elemental compositions and extracting their energetics and structural parameters into the ML model, we identified 264 energetically stable structures. Following the dynamic stability tests, 100 of these structures were found to be dynamically stable. Subsequently, we analyzed the 10 most stable structures identified in the previous step, and subjected them to more expensive phase stability tests using the evolutionary algorithm. Consequently, we succeeded in identifying five structures with dynamic, mechanical, and phase stability, which are even mechanically superior to the MAX phase counterparts derived from the late transition metals with the symmetry groups 59 (Pmmn) and 11 (P2<sub>1</sub>/m).

## 2 | DATA PREPARATION

In order to identify synthesizable LAX phases, we initially gathered a comprehensive collection of  $L_2AX$  phases, consisting of L elements exclusively from transition metals (highlighted in red in Figure 1), A-site elements primarily sourced from pnictogens, chalcogens, halogens, carbon group, boron group, and transition

metals (highlighted in blue in Figure 1), and X elements encompassing C, N, B, P, S, and Si (emphasized in blue in Figure 1). A total of 702  $L_2AX$  structures were subsequently created with orthorhombic symmetry group Pmmn (space group No. 59). The unit cells of the structures consist of eight atoms each. The structures were fully optimized in order to determine their formation energy. Notably, 54% of these structures showed negative formation energy. A positive (negative) formation energy indicates a low (high) probability of the structure being formed from isolated components.

For driving information from the structures in both MAX and LAX phase materials, the matminer<sup>60</sup> featurizer is employed (see Supporting Information 1). Furthermore, all distances between elements in components (M–A, M–X, A–X in MAX phases and L–A, L–X, and A–X in LAX phases) were extracted from the structures as the other descriptors.

## 3 | RESULTS AND DISCUSSION

The formation energies of relaxed MAX and LAX structures were analyzed in order to gain a deeper understanding of the role of elements in each structural category. The formation energies of LAX and MAX phases were calculated according to the equation:  $E_f = E_t(\text{MAX or LAX}) - 2E_t(\text{M or L}) - E_t(\text{A}) - E_t(\text{X})$ , where  $E_t(\text{MAX or LAX})$  is the total energy of MAX or LAX phases and  $E_t(\text{M or L})$ ,  $E_t(\text{A})$ , and  $E_t(\text{X})$ , are the calculated total energy of M or L, A, and X in their ground-state crystal structures. Figure S1 illustrates



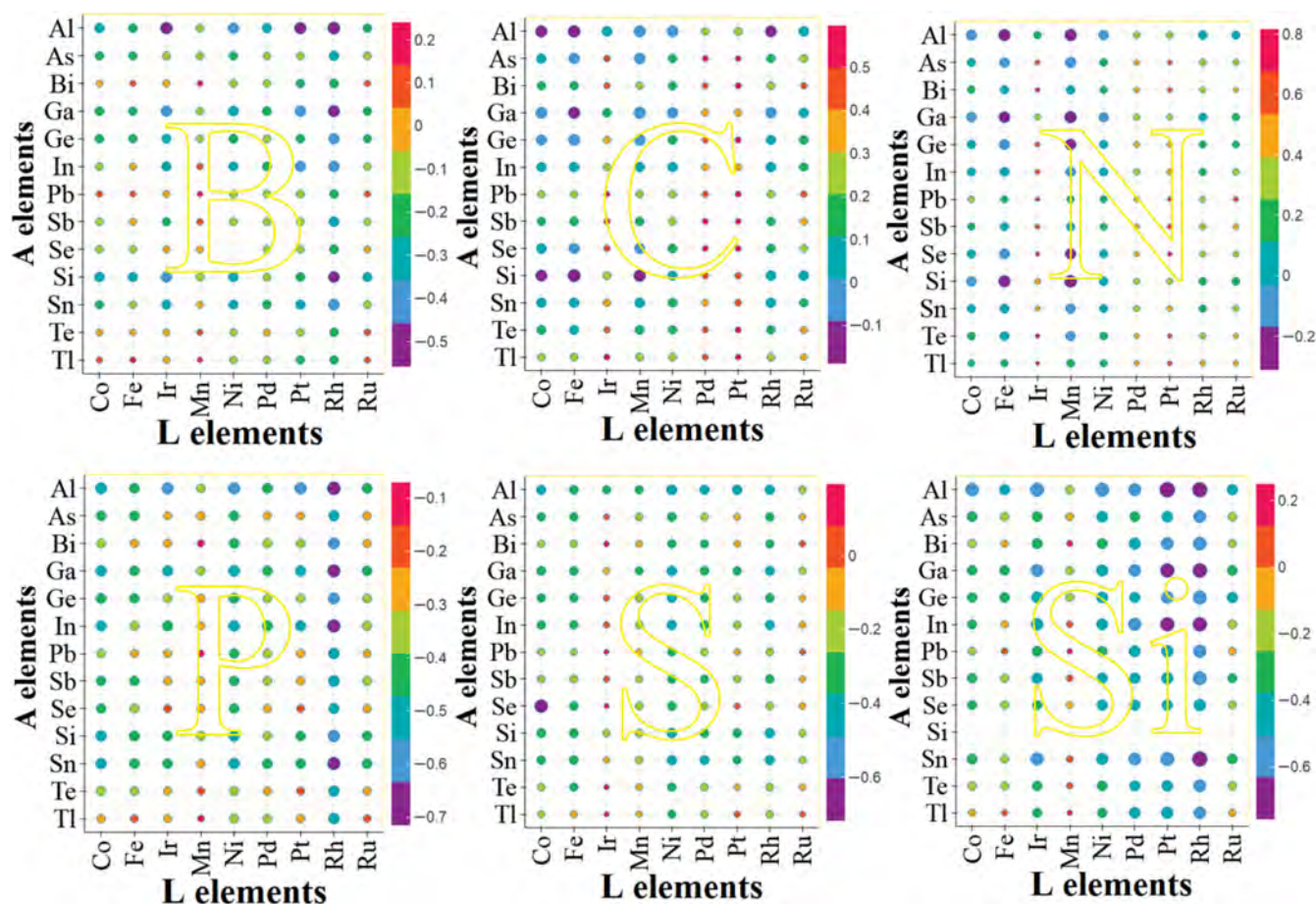
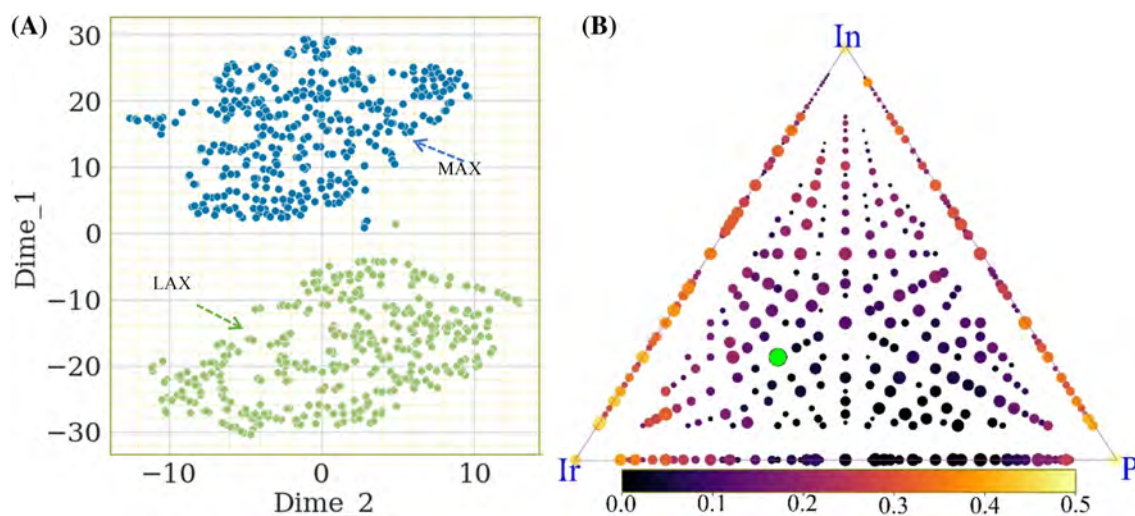


FIGURE 2 The formation energy (eV/atom) results for all 702 LAX phase structures for the X elements of boron, carbon, nitrogen, phosphor, sulfur, and silicon. Larger formation energy is depicted with large circles.

the variation in formation energy among 702 systems with similar LAX structures. In 92% of cases, the formation energies of LAX structures are more negative compared to MAX phase crystals, with only 23 exceptions (Supporting Information 1). The formation energies of LAX phases vary depending on the specific X element present. The formation energy is approximately  $-0.2$  eV/atom for the carbon and nitrogen categories, while for the other four categories, it is higher than  $-0.5$  eV/atom (Figure 2). The lower formation energies observed in ternary structures containing carbon and nitrogen can be attributed to the stability of the bonds formed by these elements and the unique bonding characteristics of other elements. Certain M elements in LAX structures, such as Pd and Ru, contribute to the formation of less stable structures based on formation energy (Figure 2). On the other hand, Rh, Pt, and Ir lead to more stable structures in boron structures containing Al. Indeed, aluminum plays a significant role in achieving more negative formation energy values in the majority of structures, with the exception of sulfides.

From a pool of 456 structures, those with negative formation energy values were selected for final screening.

Our process involves the execution of two-step calculations to classify structures as having a high likelihood of synthesis or otherwise. Initially, the formation energies of the chosen 456 systems are compared with the formation energies derived from the competing phase structures extracted from the quantum materials database (OQMD) repository. This screening methodology yields satisfactory results, as shown in previous studies.<sup>38,61</sup> In other words, we examine the relative formation energy ( $\Delta H$ ) of LAX structures in comparison to the formation energy of the most competitive phases sourced from the OQMD materials database, where  $\Delta H = E_f^{LAX} - E_f^{com}$  and  $E_f^{com}$  is the formation energy of the competing phase of binary structures. Furthermore, all the energies of the most competitive classes can be found in the open OQMD.<sup>62,63</sup> In MAX system, it has been noted that MAX phases with a maximum  $\Delta H$  of approximately  $0.12$  eV/atom have been successfully synthesized.<sup>61</sup> Therefore, in order to conduct a more comprehensive analysis of LAX compounds, we have established  $0.2$  eV/atom as the threshold for identifying LAX candidates with a high probability of synthesis (see Supporting Information 1).



**FIGURE 3** (A) The t-SNE diagram of two classes of LAX and MAX structures. (B) The convex hull diagram of  $\text{Ir}_2\text{InP}$ , where the green circle illustrates the stable structures. The range of color is in eV/atom.

Increasing the threshold value will permit to retain a greater number of compounds for the subsequent stage of our analysis, thus ensuring that no crucial LAX phase is overlooked. In the subsequent stage, we implement the ML algorithm that was efficiently crafted in our earlier computations for haeckelite configurations.<sup>56</sup> The model accurately predicted the relative formation energy in relation to the convex hull. It has been demonstrated that structures with high synthesizability have formation energies below  $E_{\text{hull}} + 0.05$  eV/atom.<sup>64,65</sup> In this process, we utilize 52 structural descriptors and implement the random forest regression model. The energy above the hull is predicted through 10-fold cross-validation using the material project datasets. The top 264 components are selected based on their superior energy above the hull. Subsequently, LAX structures that satisfy the established criteria are selected for further analysis (see [Supporting Information](#)).

We analyzed the differences between MAX and LAX structures by obtaining descriptors from 702 LAX structures and their corresponding stoichiometry compounds in MAX phases. The descriptors were classified into two categories. The first category comprised the structural information, including mass density, x-ray diffraction data, and valence band concentration of each structure. The second category involved the extrapolation of the distance between each element, which was calculated using the following equation:  $d_{ij} = (r_j - r_i)_1^n$ . In this equation,  $d$  represents the distance between elements,  $r$  is the position of each element, and  $n$  is the number of elements in the structures. A total of 162 features were generated and visualized using t-distributed stochastic neighbor embedding (t-SNE).<sup>66</sup> The application of t-SNE in this context can be extremely beneficial for uncovering complex

patterns within the dataset. Figure 3A demonstrates the excellent distribution of MAX and LAX data clusters based on these descriptors, revealing a distinct and clear separation between them. A total of 264 compounds were identified in the preceding two stages and subsequently subjected to an assessment of their dynamic stability through phonon spectra calculations (see [Supporting Information 2](#)). Out of these, 100 were found to be dynamically stable, with no imaginary phonon frequency. The structures that satisfied the stability criteria compared to competing phases, are subjected to further evaluation of phase stability using evolutionary algorithms with the USPEX code. Out of the 10 best structures identified through evolutionary algorithms search,  $\text{Ir}_2\text{InP}$ ,  $\text{Ir}_2\text{SnSi}$ , and  $\text{Pt}_2\text{GaSi}$  lie on the convex hull line.  $\text{Ni}_2\text{SnP}$  and  $\text{Ni}_2\text{InP}$  have a distance of 0.017 and 0.013 eV/atom, while the remaining five structures are situated at a distance of approximately 0.02–0.1 eV/atom from the stability line ([Supporting Information 1](#)).

The electronic band structure is considered for investigation of the electronic nature of the identified LAX phases. Figure 4A shows the calculated electronic band structure of  $\text{Ir}_2\text{InP}$ . Due to the overlapping of the conduction and valence bands, there is no band gap at the Fermi level. The Fermi level crosses the valence bands and conduction bands. The metallic behavior can be observed in all LAX structures, as shown in Figure 4 and [Supporting Information](#). The density of states (DOS) of the most stable structure, namely  $\text{Ir}_2\text{InP}$ , is predominantly influenced by the presence of Ir, as demonstrated in Figure 5A. Notably, the 5d orbitals of Ir play a significant role at the Fermi level, as evidenced by their substantial orbital contributions, as shown in Figure 4B. Furthermore, we have analyzed the partial DOS (PDOS), revealing that, apart



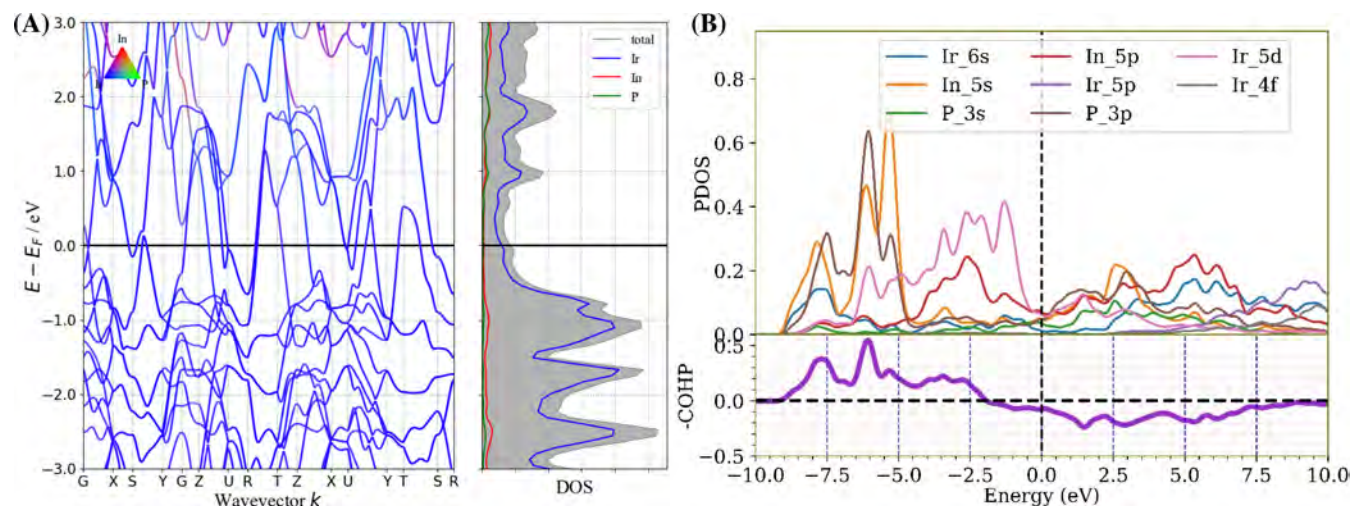


**FIGURE 4** (A) The band structure, DOS, projected DOS (PDOS (states/eV/cell)), and (B) crystal orbital Hamilton population (COHP (1/eV)) analysis for Ir<sub>2</sub>InP. The Fermi is set at zero.

from 5d(Ir), 3p(P), and 5s(In) orbitals having the most prominent contributions at the Fermi energy, other orbitals do not actively participate in the PDOS at the Fermi level. Moreover, the crystal orbital Hamilton population (COHP) analysis for Ir<sub>2</sub>InP, as illustrated in Figure 4C, demonstrates that the COHP values exhibit negativity below the Fermi energy and positivity above it. The Fermi level is situated within the COHP curve, which marks the shift from bonding to antibonding areas. This signifies the presence of solely bonding states in the respective bonds, consequently boosting the stability of the structures. As illustrated in Figure 4B, the COHP curves for Ir<sub>2</sub>InP indicates substantial antibonding interactions at the Fermi level. The conduction band (CB) is comprised of states formed by d(Ir), s(In), and p(P) orbitals up to approximately 2 eV, while the higher-energy states are predominantly derived from Iridium's 6s, 5p, and 4f orbitals. In contrast, the valence band is predominately influenced by the d(Ir) states within the energy range of −5 to 0 eV.

In order to gain a deeper insight into the mechanical stability of the final LAX phase structures, we have computed the elastic constants of the four final structures and compared them with their respective MAX phase structures. The elastic constants were determined via the strain-energy method. All five stable LAX phases satisfy the Born stability criteria, thereby signifying their mechanical robustness (see Supporting Information 1). As for the MAX phase structures, all are mechanically stable, with the exception of the Pt<sub>2</sub>GaSi structure. The mechanical characteristics of the final structures exhibit a more pronounced distinction between the LAX and MAX structures. The elastic constants have been computed and are provided in Supporting Information. These constants

provide further insights into the structures. Additional data may be obtained by employing the stiffness constants obtained. In particular, the elastic constants  $C_{11}$  and  $C_{33}$  are indicative of the solid's stiffness in the a-axis and c-axis orientations, when pressure is applied along the [100] and [001] crystallographic directions, respectively.

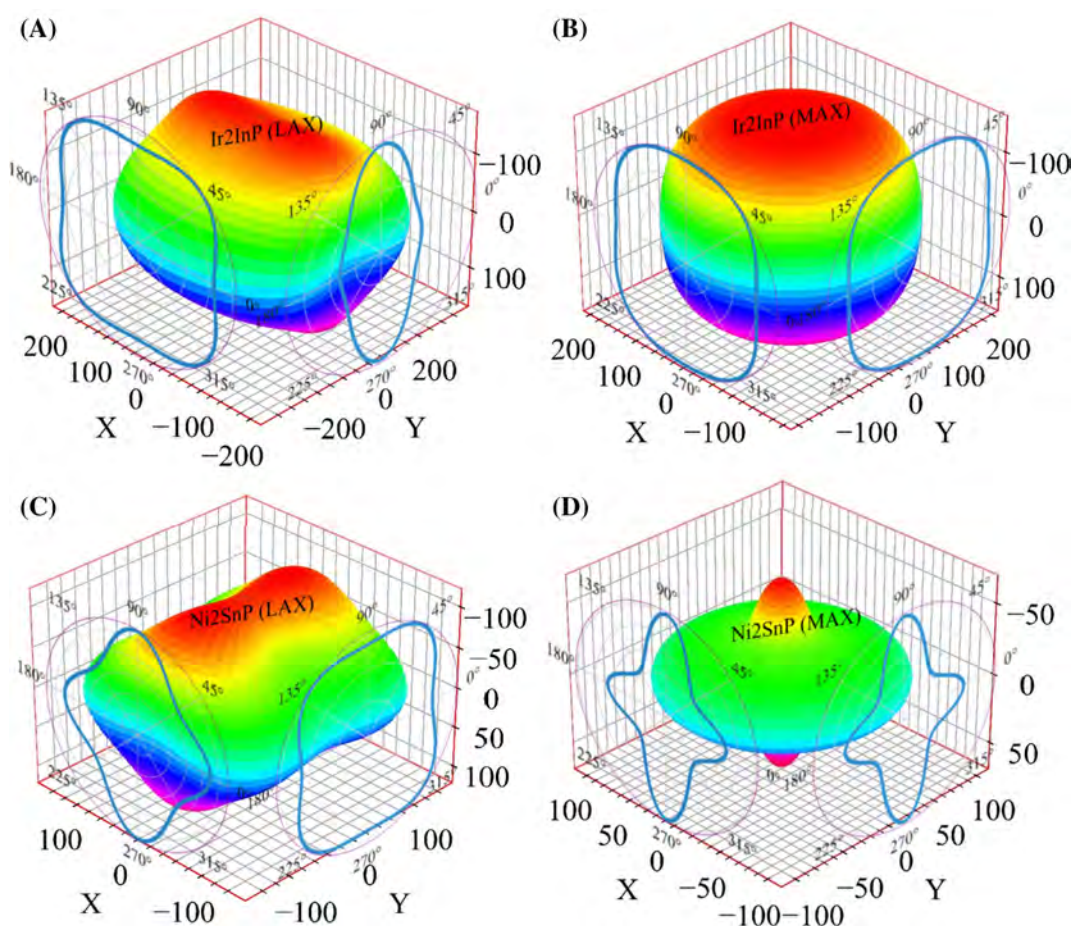
In the MAX and LAX configurations,  $C_{11}$  surpasses  $C_{33}$ , suggesting greater resistance to deformation along the ab lattices in comparison to the c-axis. Moreover, the difference between these constants highlights the anisotropic bonding strength of the configurations. In comparison to other elastic constants,  $C_{44}$  is a more reliable measure of hardness. With the exception of Ir<sub>2</sub>SnSi, all LAX configurations exhibit higher hardness values than their respective MAX phases.<sup>67</sup>

Moreover, the mechanical properties of the LAX phase exhibit significantly superior characteristics in comparison to the MAX phase. Additionally, the incorporation of late transition metals enhances interlayer bonding, contributing to enhanced stability and mechanical performance (Supporting Information 1). For instance, in the LAX phase Ni<sub>2</sub>SnSi, the Young's modulus ranges from 52.05 to 229.89 GPa with an average value of 133.13 GPa (Hill average for polycrystal). This high value indicates a significant resistance to deformation. In contrast, the Young's modulus for the MAX phase exhibits a range of 23.18 to 129.95 GPa, with an average Hill value of 59.70 GPa. This reflects a markedly lower stiffness and structural resilience. The Vickers hardness of the LAX phase is in the range of 4.10 to 5.58 GPa on average. In contrast, the MAX phase shows a lower hardness range, typically from negative values (which suggests non-ductile behavior in some samples) up to 1.84 GPa. The

**TABLE 1** The mechanical parameters of synthesizable LAX structures in comparison to their similar MAX structures.

Structure	Formula	<i>B</i> (GPa)	<i>Y</i> (GPa)	<i>S</i> (GPa)	<i>v</i> (GPa)	<i>B/G</i>	Debye (K)	VH (GPa)	Pc (GPa)	Space group number
LAX	Ir <sub>2</sub> InP	170.151	180.667	68.278	0.32	2.49	298	6.48	51.2	59
	Ir <sub>2</sub> SnSi	200.963	224.223	85.322	0.31	2.36	331.1	8.09	69.0	59
	Ni <sub>2</sub> SnP	128.485	136.071	51.406	0.32	2.50	356.1	5.283	31.5	59
	Ni <sub>2</sub> InP	136.137	127.797	47.560	0.34	2.86	343.9	4.285	47.1	59
	<b>Ni<sub>2</sub>SnSi</b>	<b>148.063</b>	<b>133.133</b>	<b>49.304</b>	<b>0.35</b>	<b>3.00</b>	<b>349.5</b>	<b>4.162</b>	<b>65.9</b>	<b>11</b>
MAX	Pt <sub>2</sub> GaSi	170.988	185.704	70.396	0.32	2.43	309.6	6.818	97.4	11
	Ir <sub>2</sub> InP	116.459	101.354	37.401	0.36	3.11	221.1	3.285	72.9	194
	Ir <sub>2</sub> SnSi	191.669	185.507	69.287	0.34	2.77	299.2	5.815	102.5	194
	Ni <sub>2</sub> SnP	98.9490	64.470	23.167	0.39	4.27	241.2	1.634	92.2	194
	Ni <sub>2</sub> SnSi	122.007	59.702	21.045	0.42	5.80	230.9	1.078	118.1	194
	Ni <sub>2</sub> InP	115.240	80.683	29.163	0.38	3.95	270.9	2.101	103.8	194

Note: The bold structure is situated at a distance of 0.038 eV/atom distance from the convex hull, while the remaining five structures are positioned along the convex energy line. Similar structures in MAX phases are unavailable due to their mechanical instability.

**FIGURE 5** The Young's modulus distribution of the two synthesizable systems of (A, B) Ir<sub>2</sub>InP and (C, D) Ni<sub>2</sub>SnP having the LAX and MAX structures.

LAX phase thus demonstrates superior wear resistance, which is essential for applications involving mechanical stress. The bulk modulus of the LAX phase ranged from

97.49 to 221.16 GPa, in comparison to the MAX phase, which spans from 55.24 to 245.96 GPa. The consistency of the LAX values indicates a more stable structure under

pressure. Similarly, the average shear modulus for LAX is 49.30 GPa, in comparison to the MAX phase, which reports values from 6.30 to 46.75 GPa, indicating an enhanced capacity to withstand shear stress in LAX. The mechanical superiority of LAX phases can be attributed to their unique layered crystal structure incorporating late transition metals, which are known for higher bonding strength and improved load-bearing capabilities. The increased anisotropy observed in LAX phases (with anisotropic ratios of 4.417 for Young's modulus in comparison to 5.605 for the MAX phase) suggests that the mechanical properties can be extensively tailored according to the loading direction, thereby offering greater flexibility in application. Similarly, this comparative analysis repeated in other final structures highlights the mechanical advantages of LAX materials. The bulk modulus and shear modulus are frequently employed to analyze how materials respond to pressure and rigidity under pressure, respectively. These moduli are employed to study pure deformations, including changes in volume and shape. According to Table 1, MAX phases have lower bulk moduli than LAX systems with similar composition, indicating the lowest resistance to hydrostatic pressure. On the other hand,  $\text{Ni}_2\text{SnP}$  demonstrates the lowest resistance to plastic deformation among the compounds under investigation. Young's modulus, represented by  $Y$ , is a measure of the rigidity of solids and establishes a relationship between this characteristic and thermal shock resistance (TSR) in an inversely proportional manner. Thus, a solid with a high  $Y$  value indicates high rigidity and low TSR. Consequently, the  $Y$  values of the LAX structures are higher than those of the MAX structures (Table 1, Figure 5). While these moduli do not directly reflect hardness, they tend to be higher for materials with greater rigidity.<sup>68</sup> Furthermore, the stiffness constants are utilized to predict whether MAX phases exhibit ductile or brittle properties by calculating Cauchy Pressure (CP). The difference between  $C_{11}$  and  $C_{44}$  represents the CP, whereby a negative or positive value indicates brittle or ductile behavior, respectively. Moreover, negative and positive values indicate the existence of directional covalent and ionic bonds, respectively. In Table 1, all MAX and LAX materials possess covalent bonds and exhibit ductile characteristics. The Vickers hardness (VH) of a solid gauges its ability to withstand deformation under extreme conditions, primarily determined by the strength of atomic bonds within the material. A variety of factors, including atomic arrangement, defects, and other related characteristics, also affect the VH of solids.<sup>69</sup> The VH of LAX structures is significantly greater, being two to three times higher than that of the MAX components. This distinction can be attributed to the bond overlap population, which is particularly

suitable for partial metallic systems. The increased VH of these structures may be attributed to the robust covalent bonding between L-X atoms, as opposed to M-X atoms. In MAX phases, the M-A bond is weaker than the covalent M-X bond due to electron interactions within the material.<sup>70–72</sup> MAX phases exhibit weaker M-A bonds than the covalent M-X bonds due to electron interactions in the material. The d electrons of M atoms interact with the s and p orbitals of X atoms, which results in strong covalent bonds in MAX structures. Conversely, the M-A bonds are predominantly metallic, leading to a weaker bond than the M-X bond. The bond distances of the M-X and M-A bonds in MAX phases are greater than those of L-X and L-A in LAX structures, indicating stronger bond strengths in LAX structures. Furthermore, the electron concentration in the structures also affects the bonding characteristics of MAX phases and, similarly, of LAX phases, influencing the filling of bonding, nonbonding, and antibonding states. A deficiency of electrons can result in partially unfilled bonding, while an excess of valence electrons can lead to overly filled antibonding states, which in turn causes instability in both cases.

## 4 | CONCLUSION

Our investigation has led to the discovery of a novel family of ternary layered transition metal compounds, designated as LAX phases. These materials present themselves as a viable alternative to MAX phase structures by incorporating late transition metals from the last groups of the d-block elements. Through utilizing advanced crystal structure prediction techniques, data-centric materials research, and the potential of ML, we have successfully identified several synthesizable LAX compounds that boast superior mechanical properties compared to traditional MAX phase materials. Our comprehensive stability evaluations, which encompass dynamic, mechanical, and phase stability in conjunction with structural characteristics, have provided a detailed insight into the potential of these innovative materials. A key distinguishable difference between the MAX and LAX structures is that when P, S, and Si are used as the X elements in combination with the last transition metals as the M elements, the stable structures converge toward the LAX systems rather than the MAX phases. Furthermore, analogous to the process of deriving MXenes from MAX phases via the chemical elimination of A elements, it is anticipated that by etching A elements from LAX phases, 2D materials, designated as LXenes, can be synthesized. It is anticipated that LXenes, like their MXene counterparts, will exhibit outstanding characteristics, including enhanced surface area and tunable electronic properties, rendering



them suitable for various energy and device technology applications. It is noteworthy that LXenes, which are composed of late transition metals, are predicted to demonstrate superior catalytic performance suitable for various catalytic applications. Late transition metals are renowned for their superior catalytic activities, highlighting their vast potential for diverse applications in catalysis. This study pushes the boundaries of existing layered materials and underscores the impact of informatics-driven material exploration in catalyzing innovation and breakthroughs in materials science. The success of our heuristic-based structure searches suggests a promising avenue for future materials discovery, paving the way for expedited exploration and creating cutting-edge materials with unparalleled properties for sophisticated applications.

## 5 | EXPERIMENTAL SECTION

In this research, we conducted first-principles calculations using the Perdew–Burke–Ernzerhof (PBE)<sup>73</sup> functional within the generalized gradient approximation (GGA) framework and the projector augmented wave method (PAW) potentials<sup>74</sup> with the Vienna Ab initio Simulation Package (VASP).<sup>75</sup> Using the conjugate gradient method, we used a plane wave cutoff energy of 520 eV to expand the wave functions and optimize atomic positions and lattice parameters. The total energy converged to a value less than 0.00001 meV/cell, and the acting force on each atom in the optimized structures was below 0.0005 eV/Å. We used fine Monkhorst–Pack<sup>76</sup> k-point meshes of  $2\pi \times 0.04 \text{ \AA}^{-1}$  to thoroughly sample the Brillouin zone for structural optimizations and total energy calculations. Furthermore, we obtained phonon dispersion spectra based on the finite displacement method using the PHONOPY code.<sup>77,78</sup> Phonon calculations utilized a  $3 \times 3 \times 1$  or  $4 \times 4 \times 1$  supercell, which provided comprehensive insight into the material's vibrational properties.

The USPEX, an evolutionary algorithm, was employed to perform structural investigations. It is a well-established software known for accurately anticipating new phases of bulk or 2D materials.<sup>79–83</sup> The minimum global structure of bulk systems, a population size of 200 individuals per generation, was employed, with the number of generations ranging from 220 to 250 based on the seed structure's contribution. In subsequent generations, a particle swarm optimization scheme determined 50% of the population from the previous generation's best structure, while the remaining 50% was randomly generated to maintain population diversity.

An ML model was utilized to examine the phase stability of structures. The Materials Project datasets were trained to predict the energy above the hull of LAX

phases using a nine-regression model with 52 descriptors. The model achieved a mean absolute error (MAE) of 0.05 eV/atom for energy above the hull, which was reported in our previous work.<sup>56</sup>

## ACKNOWLEDGMENTS

The authors sincerely thank the crew of the Center for Computational Materials Science of Institute for Materials Research, Tohoku University, for their continuous support of the supercomputing facilities (Project No. 202112-SCKXX-0501). M.K. acknowledges the support of the Iran National Science Foundation (INSF) through grant number 4025794. M.E. acknowledges the support of the JSPS Kakenhi Grant-in-Aid for Scientific Research (24K08211).

## CONFLICT OF INTEREST STATEMENT

The authors declare no conflict of interest.


## ORCID

Ehsan Alibagheri  <https://orcid.org/0009-0001-3005-3088>

Mohammad Khazaei  <https://orcid.org/0000-0001-5093-1610>

Mehdi Estili  <https://orcid.org/0000-0003-1465-8148>

Hideo Hosono  <https://orcid.org/0000-0001-9260-6728>

S. Mehdi Vaez Allaei  <https://orcid.org/0000-0002-4713-3818>

## REFERENCES

- Nowotny VH. Strukturchemie einiger Verbindungen der Übergangsmetalle mit den elementen C, Si, Ge, Sn. *Prog Solid State Chem.* 1971;5:27–70.
- Barsoum MW. The  $M_{N+1}AX_N$  phases: a new class of solids. *Prog Solid State Chem.* 2000;28(1):201–281.
- Khazaei M, Arai M, Sasaki T, Estili M, Sakka Y. Trends in electronic structures and structural properties of MAX phases: a first-principles study on  $M_2AlC$  ( $M = \text{Sc, Ti, Cr, Zr, Nb, Mo, Hf, or Ta}$ ),  $M_2AlN$ , and hypothetical  $M_2AlB$  phases. *J Phys Condens Matter.* 2014;26(50):505503.
- Zhang Z, Duan X, Jia D, Zhou Y, van der Zwaag S. On the formation mechanisms and properties of MAX phases: a review. *J Eur Ceram Soc.* 2021;41(7):3851–3878.
- Gonzalez-Julian J. Processing of MAX phases: from synthesis to applications. *J Am Ceram Soc.* 2021;104(2):659–690.
- Barsoum MW. *MAX Phases: Properties of Machinable Ternary Carbides and Nitrides.* Wiley; 2013.
- Michałowski PP, Anayee M, Mathis TS, et al. Oxycarbide MXenes and MAX phases identification using monoatomic layer-by-layer analysis with ultralow-energy secondary-ion mass spectrometry. *Nat Nanotechnol.* 2022;17(11):1192–1197.
- Li B, Wu N, Wu Q, et al. From “100%” utilization of MAX/-MXene to direct engineering of wearable, multifunctional E-textiles in extreme environments. *Adv Funct Mater.* 2023; 33(41):2307301.
- Fukamachi S, Solís-Fernández P, Kawahara K, et al. Large-area synthesis and transfer of multilayer hexagonal boron nitride

- for enhanced graphene device arrays. *Nat Electron.* 2023;6(2):126-136.
10. Chen Y, Zheng Y, Zhou Y, et al. Multi-layered cement-hydrogel composite with high toughness, low thermal conductivity, and self-healing capability. *Nat Commun.* 2023;14(1):3438.
  11. Kumar S, Kumar S. Ultrafast THz probing of nonlocal orbital current in transverse multilayer metallic heterostructures. *Nat Commun.* 2023;14(1):8185.
  12. Bae S, Kang Y-G, Khazaei M, et al. Electronic and magnetic properties of carbide MXenes—the role of electron correlations. *Mater Today Adv.* 2021;9:100118.
  13. Naguib M, Mashtalir O, Carle J, et al. Two-dimensional transition metal carbides. *ACS Nano.* 2012;6(2):1322-1331.
  14. Naguib M, Mochalin VN, Barsoum MW, Gogotsi Y. 25th anniversary article: MXenes: a new family of two-dimensional materials. *Adv Mater.* 2014;26(7):992-1005.
  15. Anasori B, Lukatskaya MR, Gogotsi Y. 2D metal carbides and nitrides (MXenes) for energy storage. *Nat Rev Mater.* 2017;2(2):1-17.
  16. Khazaei M, Ranjbar A, Esfarjani K, Bogdanovski D, Dronskowski R, Yunoki S. Insights into exfoliation possibility of MAX phases to MXenes. *Phys Chem Chem Phys.* 2018;20(13):8579-8592.
  17. Khazaei M, Ranjbar A, Arai M, Sasaki T, Yunoki S. Electronic properties and applications of MXenes: a theoretical review. *J Mater Chem C.* 2017;5(10):2488-2503.
  18. Gogotsi Y, Anasori B. The rise of MXenes. *ACS Nano.* 2019;13(8):8491-8494.
  19. Fang CM, Ahuja R, Eriksson O. Prediction of MAX phases,  $V_{N+1}SiC_N$  ( $N = 1, 2$ ), from first-principles theory. *J Appl Phys.* 2007;101(1):013511.
  20. Ahuja R. Nanolayered MAX phases from ab initio calculations. *Particle and Continuum Aspects of Mesomechanics.* Wiley; 2007:199-204.
  21. Anasori B, Xie Y, Beidaghi M, et al. Two-dimensional, ordered, double transition metals carbides (MXenes). *ACS Nano.* 2015;9(10):9507-9516.
  22. Rosen J, Dahlqvist M, Tao Q, Hultman L. In- and out-of-plane ordered MAX phases and their MXene derivatives. In: Anasori B, Gogotsi Y, eds. *2D Metal Carbides and Nitrides (MXenes).* Springer; 2019:37-52.
  23. Zhou J, Tao Q, Ahmed B, et al. High-entropy laminate metal carbide (MAX phase) and its two-dimensional derivative MXene. *Chem Mater.* 2022;34(5):2098-2106.
  24. Khazaei M, Bae S, Khaledialidusti R, et al. Superlattice MAX phases with A-layers reconstructed into 0D-clusters, 1D-chains, and 2D-lattices. *J Phys Chem C.* 2023;127(30):14906-14913.
  25. Khazaei M, Maleki I, Koshi NA, et al. Beyond metals: theoretical discovery of semiconducting MAX phases and their potential application in thermoelectrics. *Phys Chem Chem Phys.* 2024;26(27):18907-18917.
  26. Barsoum MW, Zhen T, Kalidindi SR, Radovic M, Murugaiah A. Fully reversible, dislocation-based compressive deformation of  $Ti_3SiC_2$  to 1 GPa. *Nat Mater.* 2003;2(2):107-111.
  27. El-Raghy T, Barsoum MW, Zavaliangos A, et al. Processing and mechanical properties of  $Ti_3SiC_2$ : II, effect of grain size and deformation temperature. *J Am Ceram Soc.* 1999;82(10):2855-2860.
  28. Bao YW, Zhou YC, Zhang HB. Investigation on reliability of nanolayer-grained  $Ti_3SiC_2$  via Weibull statistics. *J Mater Sci.* 2007;42(12):4470-4475.
  29. Wolfsgruber H, Nowotny H, Benesovsky F. Die Kristallstruktur von  $Ti_3GeC_2$ . *Monatshefte Für Chem.* 1967;98(6):2403-2405.
  30. Barsoum MW, El-Raghy T. The MAX phases: unique new carbide and nitride materials: ternary ceramics turn out to be surprisingly soft and machinable, yet also heat-tolerant, strong and lightweight. *Am Sci.* 2001;89(4):334-343.
  31. Sokol M, Natu V, Kota S, Barsoum MW. On the chemical diversity of the MAX phases. *Trends Chem.* 2019;1(2):210-223.
  32. Zhang Y, Mao Z, Han Q, et al. The role of Hume-Rothery's rules play in the MAX phases formability. *Materialia.* 2020;12:100810.
  33. Cover MF, Warschkow O, Bilek MMM, McKenzie DR. A comprehensive survey of M(2)AX phase elastic properties. *J Phys Condens Matter Inst Phys J.* 2009;21(30):305403.
  34. Frey NC, Wang J, Vega Bellido GI, Anasori B, Gogotsi Y, Shenoy VB. Prediction of synthesis of 2D metal carbides and nitrides (MXenes) and their precursors with positive and unlabeled machine learning. *ACS Nano.* 2019;13(3):3031-3041.
  35. Dahlqvist M, Rosen J. Predictive theoretical screening of phase stability for chemical order and disorder in quaternary 312 and 413 MAX phases. *Nanoscale.* 2020;12(2):785-794.
  36. Lukatskaya MR, Halim J, Dyatkin B, et al. Room-temperature carbide-derived carbon synthesis by electrochemical etching of MAX phases. *Angew Chem.* 2014;126(19):4977-4980.
  37. Zhang Y, Xu Y, Huang Q, et al. Structure maps for MAX phases formability revisited. *Ceram Int.* 2024;50(2, Part A):2855-2863.
  38. Dahlqvist M, Barsoum MW, Rosen J. MAX phases—past, present, and future. *Mater Today.* 2024;72:1-24.
  39. Barsoum MW, Radovic M. Elastic and mechanical properties of the MAX phases. *Annu Rev Mat Res.* 2011;41(1):195-227.
  40. Lei X, Lin N. Structure and synthesis of MAX phase materials: a brief review. *Crit Rev Solid State Mater Sci.* 2022;47(5):736-771.
  41. Wang L, Chen Q, Yang T, Guo B, Cheng Y, Xu W. Synthesis of  $(Ti_{1-x}W_x)_3SiC_2$  MAX phase solid solution and its high-temperature oxidation performance. *J Mater Sci Mater Electron.* 2022;33(22):17446-17452.
  42. Li S, Li H, Zhou Y, Zhai H. Mechanism for abnormal thermal shock behavior of  $Cr_2AlC$ . *J Eur Ceram Soc.* 2014;34(5):1083-1088.
  43. Manoun B, Gulve RP, Saxena SK, Gupta S, Barsoum MW, Zha CS. Compression behavior of  $M_2AlC$  ( $M = Ti, V, Cr, Nb$ , and  $Ta$ ) phases to above 50 GPa. *Phys Rev B.* 2006;73(2):024110.
  44. Hettinger JD, Lofland SE, Finkel P, et al. Electrical transport, thermal transport, and elastic properties of  $M_2AlC$  ( $M = Ti, Cr, Nb$ , and  $V$ ). *Phys Rev B.* 2005;72(11):115120.
  45. Sun Z, Music D, Ahuja R, Schneider JM. Theoretical investigation of the bonding and elastic properties of nanolayered ternary nitrides. *Phys Rev B.* 2005;71(19):193402.
  46. Miao N, Wang J, Gong Y, et al. Computational prediction of boron-based MAX phases and MXene derivatives. *Chem Mater.* 2020;32(16):6947-6957.
  47. Duan X, Fang Z, Yang T, et al. Maximizing the mechanical performance of  $Ti_3AlC_2$ -based MAX phases with aid of machine learning. *J Adv Ceram.* 2022;11(8):1307-1318.
  48. Mahmood A, Wang J-L. Machine learning for high performance organic solar cells: current scenario and future prospects. *Energy Environ Sci.* 2021;14(1):90-105.
  49. Lv C, Zhou X, Zhong L, et al. Machine learning: an advanced platform for materials development and state prediction in lithium-ion batteries. *Adv Mater.* 2022;34(25):2101474.

50. Kim S, Noh J, Gu GH, Aspuru-Guzik A, Jung Y. Generative adversarial networks for crystal structure prediction. *ACS Cent Sci*. 2020;6(8):1412-1420.
51. Raccuglia P, Elbert KC, Adler PDF, et al. Machine-learning-assisted materials discovery using failed experiments. *Nature*. 2016;533(7601):73-76.
52. Mortazavi B, Podryabinkin EV, Roche S, Rabczuk T, Zhuang X, Shapeev AV. Machine-learning interatomic potentials enable first-principles multiscale modeling of lattice thermal conductivity in graphene/borophene heterostructures. *Mater Horiz*. 2020;7(9):2359-2367.
53. Rajan K. Materials informatics. *Mater Today*. 2005;8(10):38-45.
54. Pilania G, Wang C, Jiang X, Rajasekaran S, Ramprasad R. Accelerating materials property predictions using machine learning. *Sci Rep*. 2013;3(1):2810.
55. Guo K, Yang Z, Yu C-H, Buehler MJ. Artificial intelligence and machine learning in design of mechanical materials. *Mater Horiz*. 2021;4(8):1153-1172.
56. Alibagheri E, Ranjbar A, Khazaei M, Kühne TD, Vaez Allaei SM. Remarkable optoelectronic characteristics of synthesizable square-octagon haeckelite structures: machine learning materials discovery. *Adv Funct Mater*. 2024;34(27):2402390.
57. Alibagheri E, Mortazavi B, Rabczuk T. Predicting the electronic and structural properties of two-dimensional materials using machine learning. *Comput Mater Contin*. 2021;67(1):1287-1300.
58. Wang D, Ivey DG. Crystal structure determination of  $\text{Ni}_2\text{InP}$ . *J Mater Sci Lett*. 1995;14(2):117-123.
59. Furuseth S, Fjellvåg H, Haaland A, Schilling BER, Volden HV. Crystal structure and properties of  $\text{Ni}_2\text{SnP}$ . *Acta Chem Scand*. 1985;39a:537-544.
60. Ward L, Dunn A, Faghaninia A, et al. Matminer: an open source toolkit for materials data mining. *Comput Mater Sci*. 2018;152:60-69.
61. Khaledialidusti R, Khazaei M, Khazaei S, Ohno K. High-throughput computational discovery of ternary-layered MAX phases and prediction of their exfoliation for formation of 2D MXenes. *Nanoscale*. 2021;13(15):7294-7307.
62. Akbarzadeh AR, Ozoliņš V, Wolverton C. First-principles determination of multicomponent hydride phase diagrams: application to the Li-Mg-N-H system. *Adv Mater*. 2007;19(20):3233-3239.
63. Kirklin S, Saal JE, Meredig B, et al. The open quantum materials database (OQMD): assessing the accuracy of DFT formation energies. *npj Comput Mater*. 2015;1(1):1-15.
64. Aykol M, Dwaraknath SS, Sun W, Persson KA. Thermodynamic limit for synthesis of metastable inorganic materials. *Sci Adv*. 2018;4(4):eaq0148.
65. Sun W, Dacek ST, Ong SP, et al. The thermodynamic scale of inorganic crystalline metastability. *Sci Adv*. 2016;2(11):e1600225.
66. van der Maaten LJP, Hinton GE. Visualizing high-dimensional data using t-SNE. *J Mach Learn Res*. 2008;9(November):2579-2605.
67. Jhi S-H, Ihm J, Louie SG, Cohen ML. Electronic mechanism of hardness enhancement in transition-metal carbonitrides. *Nature*. 1999;399(6732):132-134.
68. Ali MA, Islam AKMA, Jahan N, Karimunnesa S. First-principles study of  $\text{SnO}$  under high pressure. *Int J Mod Phys B*. 2016;30(31):1650228.
69. Tian Y, Xu B, Zhao Z. Microscopic theory of hardness and design of novel superhard crystals. *Int J Refract Met Hard Mater*. 2012;33:93-106.
70. Gou H, Hou L, Zhang J, Gao F. Pressure-induced incompressibility of ReC and effect of metallic bonding on its hardness. *Appl Phys Lett*. 2008;92(24):241901.
71. Barua P, Hossain MM, Ali MA, Uddin MM, Naqib SH, Islam AKMA. Effects of transition metals on physical properties of  $\text{M}_2\text{BC}$  ( $\text{M} = \text{V}, \text{Nb}, \text{Mo}$  and  $\text{Ta}$ ): a DFT calculation. *J Alloys Compd*. 2019;770:523-534.
72. Das P, Jahan NA, Ali M. DFT insights into Nb-based 211 MAX phase carbides:  $\text{Nb}_2\text{AC}$  ( $\text{A} = \text{Ga}, \text{Ge}, \text{Ti}, \text{Zn}, \text{P}, \text{In}$ , and  $\text{Cd}$ ). *RSC Adv*. 2023;13(8):5538-5556.
73. Perdew JP, Burke K, Ernzerhof M. Generalized gradient approximation made simple. *Phys Rev Lett*. 1996;77(18):3865-3868.
74. Kresse G, Joubert D. From ultrasoft pseudopotentials to the projector augmented-wave method. *Phys Rev B*. 1999;59(3):1758-1775.
75. Kresse G, Furthmüller J. Efficient iterative schemes for ab initio total-energy calculations using a plane-wave basis set. *Phys Rev B*. 1996;54(16):11169-11186.
76. Monkhorst HJ, Pack JD. Special points for Brillouin-zone integrations. *Phys Rev B*. 1976;13(12):5188-5192.
77. Togo A. First-principles phonon calculations with Phonopy and Phono3py. *J Physical Soc Japan*. 2023;92(1):012001.
78. Togo A, Chaput L, Tadano T, et al. Implementation strategies in phonopy and phono3py. *J Phys Condens Matter*. 2023;35(35):353001.
79. Glass CW, Oganov AR, Hansen N. USPEX—evolutionary crystal structure prediction. *Comput Phys Commun*. 2006;175(11):713-720.
80. Zhu Q, Li L, Oganov AR, Allen PB. Evolutionary method for predicting surface reconstructions with variable stoichiometry. *Phys Rev B*. 2013;87(19):195317.
81. Hu C-H, Oganov AR, Zhu Q, et al. Pressure-induced stabilization and insulator-superconductor transition of BH. *Phys Rev Lett*. 2013;110(16):165504.
82. Zhou X-F, Oganov AR, Qian G-R, Zhu Q. First-principles determination of the structure of magnesium borohydride. *Phys Rev Lett*. 2012;109(24):245503.
83. Popov ZI, Tikhomirova KA, Demin VA, et al. Novel two-dimensional boron oxynitride predicted using the USPEX evolutionary algorithm. *Phys Chem Chem Phys*. 2021;23(46):26178-26184.

## SUPPORTING INFORMATION

Additional supporting information can be found online in the Supporting Information section at the end of this article.

**How to cite this article:** Alibagheri E, Khazaei M, Estili M, et al. LAX phases: A family of novel stable layered materials, informatics-based discovery. *InfoMat*. 2025;e12664. doi:[10.1002/inf2.12664](https://doi.org/10.1002/inf2.12664)